Available online at www.sciencedirect.com

ScienceDirect

IFAC Papers Online CONFERENCE PAPER ARCHIVE

IFAC PapersOnLine 50-1 (2017) 3449–3454

Nonlinear State Estimation for Trajectory Tracking of a Flexible Parallel Manipulator ⋆

Merlin Morlock * **Christian Schröck Markus Burkhardt** ** **Robert Seifried** *

* *Institute of Mechanics and Ocean Engineering, Hamburg University of Technology (TUHH), 21073 Hamburg, Germany (e-mail: robert.seifried@tuhh.de)*

** *Institute of Engineering and Computational Mechanics, University of Stuttgart, 70569 Stuttgart, Germany*

Abstract: Lightweight robots can be advantageous when considering the lower energy consumption, the possibility to use smaller motors and the lower material cost. Nevertheless, in such lightweight structures non-negligible flexibilities are inherent which can lead to significant oscillations making the control more difficult. Within this research end-effector trajectory tracking of a parallel manipulator with a highly flexible link is considered. As centerpiece, a new approach to estimate the state of the system of differential algebraic equations is discussed to obtain the end-effector position and velocity. For the estimator, the kinematic loop is treated by a projection tangential to the constraint manifold which is based on a QR decomposition. Subsequently, an Unscented Kalman Filter is applied and the dependent coordinates are obtained by satisfying the algebraic constraint equations with the Newton-Raphson method. The utilized signals for the estimator are on the one hand position measurements of the actuators which are realized as direct drives and on the other hand measurements of strain gauges attached to the long and highly flexible link. As application, a basic end-effector output controller based on an equivalent rigid model and the transfer function of the dominant first bending eigenmode is utilized to enhance the tracking results. The concepts are applied to an experimental rig for validation purposes and to show first results for end-effector estimation with feedback control.

Keywords: nonlinear state estimation, trajectory tracking, flexible arms, kinematic loop, differential algebraic equations, output feedback

1. INTRODUCTION

Flexible manipulators are highly interesting as they allow to save energy as well as material cost and they can provide increased safety in the case of human-machine interaction. However, severe undesired oscillations can occur which drastically limit their accuracy and even might cause harm. To prevent such a scenario, the overall objective of the presented research is to keep the end-effector of a flexible parallel manipulator on a defined trajectory. This has been successfully realized by feedforward control based on the inverse dynamics of the full dynamic flexible model by using servo-constraints. Thereby, a two-point boundary value problem has to be solved due to the unstable internal dynamics (Burkhardt et al., 2015; Morlock et al., 2016).
In order to further improve the end-effector tracking performance, the tracking error needs to be controlled in a feedback loop. So far, the measured actuator positions and link curvatures as well as the corresponding time derivatives have only been used to control themselves (Morlock et al., 2015, 2016). Thus, it is necessary to measure or estimate the end-effector point online in order to use it for such a feedback control. As direct measurements with high-speed cameras typically have significant time delays and laser tracking is very expensive, a nonlinear state estimator is introduced based on the available measurements. This estimator makes use of the well-known Unscented Kalman Filter (UKF; Thrun et al. (2005)), but with an adaption for flexible multibody systems with algebraic constraint equations extending the methods in the related literature (e.g. Teixeira et al. (2009)). The approach within this research uses minimal coordinates for the UKF as Pastorino et al. (2013) but by utilizing a projection based on a QR decomposition and the constraints are satisfied with the Newton-Raphson method. Furthermore, a basic feedback controller is introduced using the end-effector estimation in order to reduce the tracking error of the flexible system. The proposed controller is based on the kinematics of an equivalent rigid model, but with an additional compensation of the first bending eigenmode. Experiments are conducted validating the discussed concepts.
This research is organized in the following way: in sections 2 and 3 the considered system is described and modeled. In section 4 the nonlinear state estimator is designed. And finally, in section 5 the end-effector feedback controller is

⋆ The authors would like to thank the German Research Foundation (DFG) for their financial support of the project SE1685/3-2.

10.1016/j.ifacol.2017.08.846

introduced and applied together with the estimator to an experimental rig.

2. CONSIDERED SYSTEM

The investigated system is depicted in Fig. 1 which is designed to be highly flexible in order to test the performance of the developed control methods. Here, two 2 mm thin and elastic steel links are mounted on two parallel linear direct drives and connected to each other with a revolute joint. Since the shorter link exhibits only negligible oscillations it is considered to be rigid. The longer link with a length of approximately one meter however can show significant vibration amplitudes being visualized by a red double-headed arrow indicating a typical oscillation scenario. The inertial system xyz is used to describe the motion which occurs in the xy-plane. Moreover, as we have a connection of both links a kinematic loop is introduced.
Measurements are performed with encoders on the actuators in order to obtain the position of their center points s_1 and s_2, each having a range of motion of $\pm 30\,\text{cm}$. Note that within this research, the fixed numbers 1 and 2 in an index depict the related actuator. Additionally, strain gauges in Wheatstone bridge circuits are applied at three different locations on the long link to obtain the curvature at different positions. At the end of the long link an end-effector mass is attached with two reflective markers for video tracking with the inner marker representing the end-effector point. A camera is mounted vertically over the experimental rig and can be used for an offline image processing to identify the tracking error. Besides not being real-time capable the utilized image processing is not automatically synchronized to the time stamps of the real-time system. These drawbacks can be easily overcome by an estimator based on actuator positions and strain measurements, see section 4. For more details on the experimental rig it is pointed to Burkhardt et al. (2015) and Morlock et al. (2016).

3. FLEXIBLE MULTIBODY SYSTEM MODEL

As there are significant and uncertain friction forces within the actuators (Morlock et al., 2015), the linear drives are modeled as position actuators instead of using the motor currents as input. This is meaningful on the one hand for a state estimation since the actuator position measurements

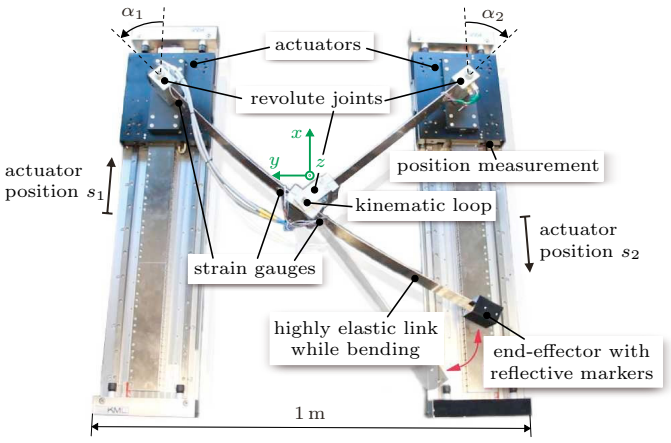

Fig. 1. Experimental rig of the parallel manipulator.

are very accurate and thus deliver precise inputs to an estimator model. On the other hand for controlling the long link a calculation of the necessary actuator motion is advantageous since the corresponding cascade controllers are able to accurately realize such a desired movement in spite of the friction. Thus, the drive positions s_1 and s_2 are not considered as degrees of freedom but as rheonomic constraints. For the modeling of the flexible multibody system the floating frame of reference approach is used (Shabana, 1997). Furthermore, as discussed in Burkhardt et al. (2015) the kinematic loop is cut open in order to describe the resulting system in tree structure with the coordinates $\boldsymbol{q} \in \mathbb{R}^f$ consisting of the two angles α_1 and α_2 as well as of the elastic coordinates $\boldsymbol{q}_\text{e}$ of the long link. The latter ones come from a reduction of the corresponding finite element model which consists of 200 BEAM188 elements modeled with ANSYS. By closing the kinematic loop two constraints occur for the considered planar system. Thus, one obtains $f-2$ independent as well as two dependent coordinates. In analogy to Seifried et al. (2013) the forward dynamics of the flexible multibody system can then be described by

$$\boldsymbol{M}\ddot{\boldsymbol{q}} = \boldsymbol{f} + \boldsymbol{B}\boldsymbol{u} + \boldsymbol{C}^\text{T}\boldsymbol{\lambda}, \tag{1a}$$

$$\boldsymbol{0} = \boldsymbol{c}. \tag{1b}$$

Due to the kinematic loop described by the closing constraints $\boldsymbol{c} = \boldsymbol{0} \in \mathbb{R}^2$ the equations of motion represent a system of differential algebraic equations (DAEs) with bold capital letters being matrices, bold lower case letters representing vectors and letters which are not bold are scalars. Moreover, $\boldsymbol{M}$ is the mass matrix and $\boldsymbol{B}$ is the input matrix of the controls. Additionally, $\boldsymbol{f}$ is the force vector containing the centrifugal, the Coriolis and the gyroscopic forces as well as applied forces which are not related to the control inputs $\boldsymbol{u}$, being the actuator accelerations. Furthermore, the Jacobian matrix of the constraints is denoted by $\boldsymbol{C}$ and $\boldsymbol{\lambda}$ are the corresponding Lagrange multipliers, i.e. the cut joint reaction forces (Seifried, 2014). Please note that the equations of motion (1) also depend on the actuator positions s_1 and s_2 as well as their corresponding time derivatives.

4. NONLINEAR STATE ESTIMATOR

In this section a nonlinear estimator is introduced to estimate the system state for the set of DAEs (1). The results can then be used to obtain the end-effector position and velocity. For the estimator a UKF framework is chosen because of its ability to handle noisy measurements and since it is well-suited for real-time estimation for nonlinear systems as Kalman algorithms are not computationally expensive (Marafioti et al., 2009). Moreover, according to Wan and Van Der Merwe (2000) the UKF is typically more accurate than the Extended Kalman Filter while sharing a similar level of complexity.

4.1 Design of the Nonlinear State Estimator

The main idea within the estimator is to transform the DAEs (1) into minimal coordinates (Pastorino et al., 2013), i.e. ordinary differential equations. This is performed in each time step by a projection based on a QR decomposition. For the UKF, this projection reduces the necessary

sigma points and it prevents a sigma point generation that violates the algebraic constraints. In such a case corrections would be necessary which increase the computational time. Subsequently, for the minimal coordinates a common UKF is utilized. Finally, the dependent coordinates are obtained by closing the kinematic loop through satisfying the constraint equations with the Newton-Raphson method in each time step.

First, the observability is checked for the considered system. Since the drives' kinematics is used as input, the only outputs are the curvature measurements $\boldsymbol{\kappa}$. Here, a linear relationship between the curvatures κ_i at the different measurement points and the elastic coordinates $\boldsymbol{q}_\mathrm{e}$ exists

$$\kappa_i = \underbrace{\frac{\partial \boldsymbol{\Psi}_z}{\partial \ell}\Big|_{\ell_i}}_{\boldsymbol{C}_{\kappa,i}} \boldsymbol{q}_\mathrm{e}, \tag{2}$$

with $\boldsymbol{\Psi}_z$ being the rotational shape functions. Their change over the beam length is evaluated at the positions ℓ_i of the strain gauges. In case of using as many strain gauges as elastic coordinates in the model, the sensor positions can be chosen such that within the linear relation

$$\boldsymbol{\kappa} = \boldsymbol{C}_\kappa \boldsymbol{q}_\mathrm{e}, \tag{3}$$

the constant output matrix $\boldsymbol{C}_\kappa$ has full rank. This means that its inverse can be obtained in order to calculate the elastic coordinates from the outputs. Also, the angles α_1 and α_2 of the links can be reconstructed from the constraint equations together with the actuator kinematics. Thus, the full state can be obtained leading to observability in all feasible system configurations.

Next, the estimator is designed. Following Seifried et al. (2013), a QR decomposition is applied to the transposed Jacobian matrix $\boldsymbol{C}$ of the constraints leading to

$$\boldsymbol{C}^\mathrm{T} = [\boldsymbol{Q}_\mathrm{c} \ \boldsymbol{J}_\mathrm{c}] \begin{bmatrix} \boldsymbol{R}_\mathrm{c} \\ \boldsymbol{0} \end{bmatrix} = \boldsymbol{Q}_\mathrm{c} \boldsymbol{R}_\mathrm{c}. \tag{4}$$

With the time derivatives of the constraints

$$\dot{\boldsymbol{c}} = \frac{\partial \boldsymbol{c}}{\partial \boldsymbol{q}} \dot{\boldsymbol{q}} + \frac{\partial \boldsymbol{c}}{\partial t} = \boldsymbol{C}\dot{\boldsymbol{q}} + \boldsymbol{c}' = \boldsymbol{0}, \tag{5a}$$

$$\ddot{\boldsymbol{c}} = \boldsymbol{C}\ddot{\boldsymbol{q}} + \boldsymbol{c}'' = \boldsymbol{0}, \tag{5b}$$

the equations of motion in minimal form follow by a projection tangential to the constraint manifold as

$$\dot{\boldsymbol{\xi}} = \boldsymbol{J}_\mathrm{c}^\mathrm{T}(\dot{\boldsymbol{q}} + \boldsymbol{Q}_\mathrm{c}\boldsymbol{R}_\mathrm{c}^{-\mathrm{T}}\boldsymbol{c}'), \tag{6a}$$

$$\ddot{\boldsymbol{\xi}} = \left(\boldsymbol{J}_\mathrm{c}^\mathrm{T}\boldsymbol{M}\boldsymbol{J}_\mathrm{c}\right)^{-1} \boldsymbol{J}_\mathrm{c}^\mathrm{T}(\boldsymbol{f} + \boldsymbol{B}\boldsymbol{u} + \boldsymbol{M}\boldsymbol{Q}_\mathrm{c}\boldsymbol{R}_\mathrm{c}^{-\mathrm{T}}\boldsymbol{c}''), \tag{6b}$$

for the new independent coordinates $\boldsymbol{\xi} \in \mathbb{R}^{f-2}$. Following the local coordinate algorithm of Hairer et al. (2006) the coordinates $\boldsymbol{q}$ and $\dot{\boldsymbol{q}}$ can be decomposed as

$$\underbrace{\begin{bmatrix} \boldsymbol{q} \\ \dot{\boldsymbol{q}} \end{bmatrix}}_{\boldsymbol{x}} = \underbrace{\begin{bmatrix} \boldsymbol{q}_0 \\ \dot{\boldsymbol{q}}_0 \end{bmatrix}}_{\boldsymbol{x}_0} + \underbrace{\begin{bmatrix} \boldsymbol{J}_\mathrm{c} & \boldsymbol{0} \\ \boldsymbol{0} & \boldsymbol{J}_\mathrm{c} \end{bmatrix}}_{\tilde{\boldsymbol{J}}_\mathrm{c}} \underbrace{\begin{bmatrix} \boldsymbol{\xi} \\ \dot{\boldsymbol{\xi}} \end{bmatrix}}_{\boldsymbol{z}} + \underbrace{\begin{bmatrix} \boldsymbol{Q}_\mathrm{c} & \boldsymbol{0} \\ \boldsymbol{0} & \boldsymbol{Q}_\mathrm{c} \end{bmatrix}}_{\tilde{\boldsymbol{Q}}_\mathrm{c}} \underbrace{\begin{bmatrix} \boldsymbol{\eta} \\ \dot{\boldsymbol{\eta}} \end{bmatrix}}_{\boldsymbol{n}}, \tag{7}$$

with $\boldsymbol{n} \in \mathbb{R}^4$ and $\boldsymbol{z}$ being the local coordinates. In the estimator, the start value $\boldsymbol{x}_0$ represents $\hat{\boldsymbol{x}}_{k-1}^+$ with the plus denoting a posterior quantity, $k-1$ being the last time step before the current k and the hat symbol represents an estimated quantity. A minus would describe a prior quantity. With the error covariance matrix $\boldsymbol{P}_{zz,k-1}^+$ of the last time step the origin-centered sigma points $\boldsymbol{\mathcal{Z}}_{k-1}$ are generated in $\boldsymbol{z}$-coordinates, with bold calligraphic letters representing vectors. Based on (7) the results are then plugged into

$$\boldsymbol{\mathcal{X}}_{i,k-1} = \hat{\boldsymbol{x}}_{k-1}^+ + \tilde{\boldsymbol{J}}_\mathrm{c}\boldsymbol{\mathcal{Z}}_{i,k-1}, \tag{8}$$

which is used to calculate (6). The results are then integrated with a forward Euler step to obtain $\bar{\boldsymbol{\mathcal{Z}}}_{i,k}^*$ for each sigma point, denoted by i. Now, in accordance with the usual UKF algorithm (see e.g. Thrun et al. (2005)) the prior mean $\hat{\boldsymbol{z}}_k^-$ is obtained and utilized to calculate the prior error covariance matrix $\boldsymbol{P}_{zz,k}^-$. Thereby, the new sigma points $\bar{\boldsymbol{\mathcal{Z}}}_k$ can be generated. Analog to (8)

$$\bar{\boldsymbol{\mathcal{X}}}_{i,k} = \hat{\boldsymbol{x}}_{k-1}^+ + \tilde{\boldsymbol{J}}_\mathrm{c}\bar{\boldsymbol{\mathcal{Z}}}_{i,k} \tag{9}$$

is then used within the output function $\boldsymbol{h}$ for the curvature

$$\bar{\boldsymbol{\mathcal{Y}}}_{i,k} = \boldsymbol{h}(\bar{\boldsymbol{\mathcal{X}}}_{i,k}). \tag{10}$$

The following necessary steps are the remaining standard UKF calculations but applied to the independent coordinates from which the posterior quantities $\hat{\boldsymbol{z}}_k^+$ and $\boldsymbol{P}_{zz,k}^+$ are obtained. Based on this, the starting value

$$\hat{\boldsymbol{x}}_{k,0}^+ = \hat{\boldsymbol{x}}_{k-1}^+ + \tilde{\boldsymbol{J}}_\mathrm{c}\hat{\boldsymbol{z}}_k^+ \tag{11}$$

can be found. The result is then used within the Newton-Raphson method in order to fulfill the algebraic constraints on position (1b) and velocity level (5a). This yields the relations

$$\boldsymbol{\eta}_n = -\boldsymbol{R}_\mathrm{c}^{-\mathrm{T}}\boldsymbol{c}(t, \hat{\boldsymbol{q}}_{k,n-1}^+), \tag{12a}$$

$$\dot{\boldsymbol{\eta}}_n = -\boldsymbol{R}_\mathrm{c}^{-\mathrm{T}}\dot{\boldsymbol{c}}(t, \hat{\boldsymbol{q}}_{k,n-1}^+, \hat{\dot{\boldsymbol{q}}}_{k,n-1}^+), \tag{12b}$$

with

$$\hat{\boldsymbol{q}}_{k,n}^+ = \hat{\boldsymbol{q}}_{k,n-1}^+ + \boldsymbol{Q}_\mathrm{c}\boldsymbol{\eta}_n, \tag{13a}$$

$$\hat{\dot{\boldsymbol{q}}}_{k,n}^+ = \hat{\dot{\boldsymbol{q}}}_{k,n-1}^+ + \boldsymbol{Q}_\mathrm{c}\dot{\boldsymbol{\eta}}_n \tag{13b}$$

and n denoting the iteration step while t is the time. Typically the algorithm converges fast delivering very accurate results for few steps of the projection on the considered constraints. Finally, the end-effector position and velocity can be calculated from the estimated states.

In Fig. 2, the algorithm is visualized. Here, $\boldsymbol{Q}_k$ and $\boldsymbol{R}_k$ denote the process and the measurement noise covariance matrices which are sources of additive Gaussian white noise. Moreover, $\boldsymbol{u}_k$ represents the actuator accelerations and $\boldsymbol{y}_k$ the curvature measurements, whereas $\boldsymbol{s}_k$ and $\dot{\boldsymbol{s}}_k$ are the current actuator positions and velocities.

While the reduction of the degrees of freedom by modeling the drives as position actuators has advantages, it shifts the problem of estimating the kinematic actuator quantities to another filter. However, this one can be designed in a much simpler way also since very accurate and smooth position measurements are available. Here, the motion of each actuator is considered independently as a single degree of freedom system. The neglected dynamics is represented by process noise. Based on Singer (1970) who describes the acceleration with a stationary Markov process of first order, the discrete equations of motion of each drive can be written as

$$\begin{bmatrix} s_k \\ \dot{s}_k \\ \ddot{s}_k \end{bmatrix} = \begin{bmatrix} 1 & T & (\alpha T - 1 + \mathrm{e}^{-\alpha T})/\alpha^2 \\ 0 & 1 & (1 - \mathrm{e}^{-\alpha T})/\alpha \\ 0 & 0 & \mathrm{e}^{-\alpha T} \end{bmatrix} \begin{bmatrix} s_{k-1} \\ \dot{s}_{k-1} \\ \ddot{s}_{k-1} \end{bmatrix} + \boldsymbol{w}_{k-1}, \tag{14}$$

$$y_{\mathrm{s},k} = s_k + v_k. \tag{15}$$

Here, s_k is again the current actuator position with v_k being Gaussian white noise. Additionally, $\boldsymbol{w}_{k-1}$ can be

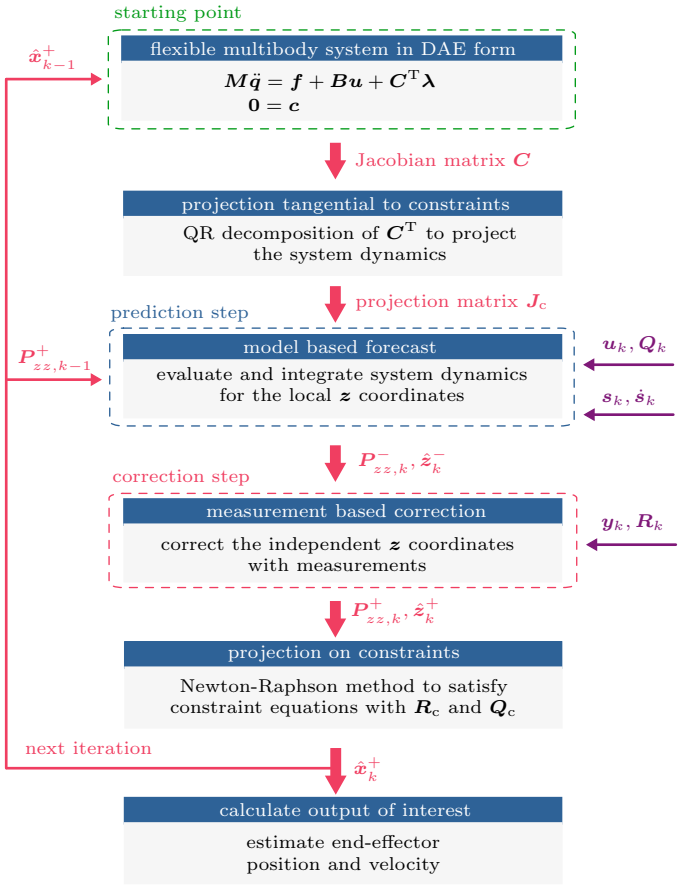

Fig. 2. Overview of the algorithm of the UKF for flexible multibody systems in DAE form.

found in Singer (1970) which is a discrete time white noise sequence being a function of the parameter α here chosen empirically to 10/7 and of T being the sample time. The term $y_{s,k}$ is the system output. A UKF algorithm is used again for state estimation. It turns out that the introduced estimators perform sufficiently fast to run in real-time on the experimental rig at $T = 0.25\,\text{ms}$.

Since within an experiment it is difficult to measure higher order modes and as the estimation has to be real-time capable the estimator will use a model which is based only on the first bending eigenmode of the long link, i.e. $\boldsymbol{q}_e \in \mathbb{R}^1$. In order to justify this simplification, a comparison is performed to a model with six elastic degrees of freedom, obtained from a hybrid Craig-Bampton/Gramian-matrix-based model-order reduction (Burkhardt et al., 2013). For more information on the mode shapes and corresponding frequencies it is pointed to Burkhardt et al. (2015).

To compare both models, a straight line shall be followed in 0.5 s as desired end-effector motion, see Fig. 3b), representing a typical application scenario. This trajectory is used within the inverse dynamics of an equivalent rigid model to obtain feedforward actuator trajectories, which are then used as input. This feedforward control will also be used as a basis for all further investigations. The reason is that it can be calculated in real-time in contrast to the elastic model offering the possibility to generate the desired end-effector trajectory online and it is well-suited to investigate the considered concepts. The results in Fig. 3a) of the root mean square (rms) and the maximum (max) end-effector position deviation norm show

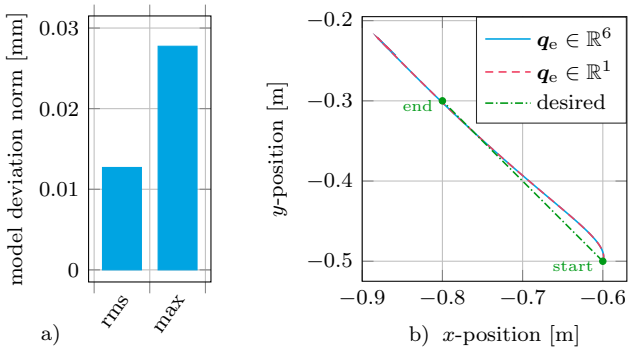

Fig. 3. Simulated a) Euclidean norm of the end-effector tracking deviation between the model with one and six elastic degrees of freedom and b) corresponding path plots for the line trajectory.

that the model differences are very small compared to the overall motion of multiple centimeters. This is confirmed by Fig. 3b). Moreover, the error is negligible compared to the experimental tracking errors presented in Morlock et al. (2016). This justifies the use of a one elastic degree of freedom model being based on a single strain gauge position. Here, the middle of the three strain gauge positions of Fig. 1 is utilized.

4.2 Validation of the Nonlinear State Estimator

The estimator is validated with experimental data at which the feedforward actuator trajectories are realized with cascade controllers (Morlock et al., 2016). Note that a theoretical validation goes beyond the scope of this research. Within Fig. 4, the filtering of the curvature can be investigated. In Fig. 4a) one can see that the measured curvature is relatively noisy compared to the estimated signal. Also, it can be observed that there is an undesired offset of the zero-point of the strain gauges (which changes throughout the measurements) that is reduced by the filter. Within the actual trajectory going from 1 s to 1.5 s in Fig. 4b), the measured signal jumps at around 1.43 s being outliers which are also smoothened by the filter. This will finally help to obtain better end-effector estimations. Besides, the simulated curvature is mostly in accordance with the measurements and the constraint equations are fulfilled up to numerical errors for four steps of the Newton-Raphson method (see Fig. 2).

Figure 5a) shows the end-effector tracking error which is on the one hand estimated by the filter and on the other hand measured using a camera. The error magnitudes are comparable but also differences of several millimeters are possible. These result from using completely different sensor sets, strain gauges and a camera, with the former being an indirect way and the latter being a direct way to obtain the end-effector position. Moreover, both utilized sensor sets perform not very accurate at this experimental rig leading to end-effector position errors that can be in the order of millimeters in a worst case scenario. Another source of error is that for the flexible beam the assumption of geometric linearity is used. However, for this example trajectory the maximal deformation becomes relatively large which violates this assumption. This behavior can be observed in Fig. 5b) when overshooting the end point, where the deviation between camera measurement and estimator rises.

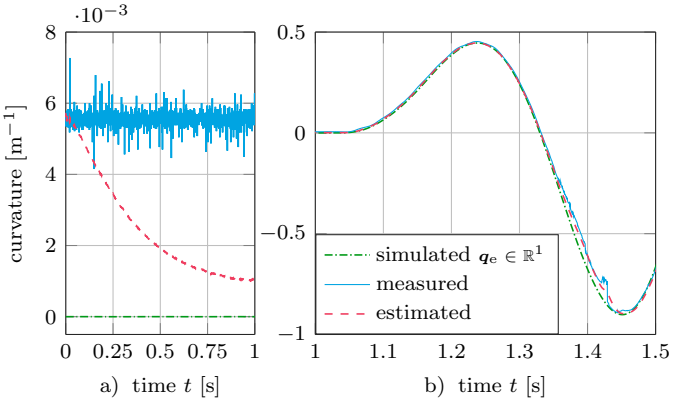

Fig. 4. Curvature for the line trajectory for a) a magnification of the starting phase and b) the tracking scenario.

Nevertheless, the estimator produces meaningful results for cases with moderate deformations in which an accuracy of some millimeters is sufficient. In contrast to the offline image processing the end-effector data is consequently available in real-time and can be used within a controller. The need for such a controller is confirmed by the large tracking deviations from the desired end-effector motion.

5. END-EFFECTOR FEEDBACK CONTROLLER

The state estimator shall be used within a basic controller in order to obtain first results for end-effector feedback control. The overall control structure can be seen in Morlock et al. (2016), to which the block diagram of Fig. 6 is added. It contains the estimator and the end-effector feedback controller being explained in the following.

The aim is to calculate the needed position and velocity corrections s_c and $\dot{s}_\mathrm{c}$ of each actuator in order to decrease the end-effector trajectory tracking error. To obtain these terms, the relation between the end-effector accelerations $\ddot{\varepsilon}_x$ in x-direction as well as $\ddot{\varepsilon}_y$ in y-direction and the actuator kinematics is used which can be written as

$$\begin{bmatrix}\ddot{\varepsilon}_x\\ \ddot{\varepsilon}_y\end{bmatrix} = \boldsymbol{d}_\mathrm{nl}(s_1, s_2, \dot{s}_1, \dot{s}_2, \ddot{s}_1, \ddot{s}_2), \tag{16}$$

for an equivalent rigid model. As the function $\boldsymbol{d}_\mathrm{nl}$ is nonlinear and the relation cannot be inverted uniquely a linearization is performed at 101 points with different

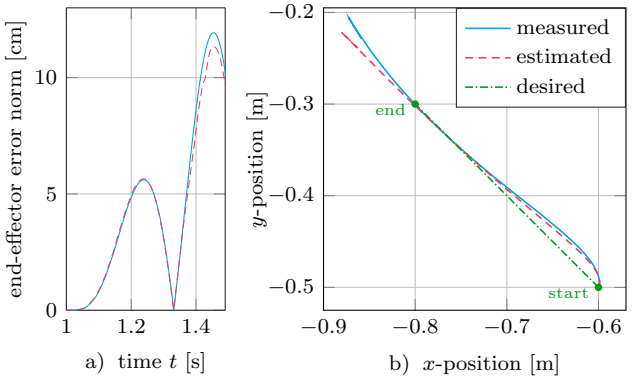

Fig. 5. Estimated and measured a) Euclidean end-effector trajectory tracking error norm and b) path plots for the line trajectory.

actuator positions s_1 and s_2 and corresponding time derivatives of zero, leading to the linear formula

$$\begin{bmatrix}\ddot{\varepsilon}_x\\ \ddot{\varepsilon}_y\end{bmatrix} = \boldsymbol{D}_\mathrm{r}\begin{bmatrix}\ddot{s}_1\\ \ddot{s}_2\end{bmatrix}. \tag{17}$$

Here, $\boldsymbol{D}_\mathrm{r}$ is the feedthrough matrix at the considered working point. This kinematic relation can then be used to minimize the end-effector tracking error by applying the actuator accelerations of

$$\begin{bmatrix}\ddot{s}_1\\ \ddot{s}_2\end{bmatrix} = \boldsymbol{D}_\mathrm{r}^{-1}\begin{bmatrix}\ddot{\varepsilon}_{x,\mathrm{d}} + D(\dot{\varepsilon}_{x,\mathrm{d}} - \dot{\varepsilon}_x) + P(\varepsilon_{x,\mathrm{d}} - \varepsilon_x)\\ \ddot{\varepsilon}_{y,\mathrm{d}} + D(\dot{\varepsilon}_{y,\mathrm{d}} - \dot{\varepsilon}_y) + P(\varepsilon_{y,\mathrm{d}} - \varepsilon_y)\end{bmatrix}, \tag{18}$$

where the index "d" denotes desired. Thus, with the gains $P, D > 0$ one obtains two decoupled and stable dynamic equations for both end-effector coordinates. Note that the corresponding desired accelerations $\ddot{\varepsilon}_{x,\mathrm{d}}$ and $\ddot{\varepsilon}_{y,\mathrm{d}}$ are covered by the feedforward controller.

This feedback controller works well for the rigid model as well as for a collocated (rigid) output in the elastic case but it destabilizes the system if the end-effector point is chosen as output in an elastic case. Therefore, the first and dominant bending eigenmode is roughly compensated by applying its inverse transfer function to the feedback signals. An additional filtering is performed by a tuned second order transfer function with two complex poles to obtain amongst others a proper overall transfer function. The compensation then reads as follows

$$G_\mathrm{c}(S) = \frac{\frac{1}{246.1}S^2 + \frac{0.228}{246.1}S + 1}{\frac{1}{1000}S^2 + \frac{33}{1000}S + 1}. \tag{19}$$

Here, S is the complex frequency parameter of the Laplace transform. In the diagram of Fig. 6, besides the already explained blocks a high-pass filter is used to further reduce the nonphysical measurement offset within the strain gauges. This offset has a dominant effect on the end-effector velocity estimation which might lead to wrong feedback control actions. Consequently, another high-pass filter is used to minimize the occurring drift in the estimated velocity error. Furthermore, the actuator acceleration corrections a_c1 and a_c2 are sent to an additional high-pass filter, being taken from Morlock et al. (2015). It prevents e.g. unwanted drifts in the filtered position corrections s_c1 and s_c2 after turning the controller off. The filtered position and velocity signals are then used within the cascade controllers to change the desired actuator motions.

Experiments are conducted for the line trajectory being illustrated in Fig. 7. The utilized controller parameters are $P = 5\,\mathrm{s}^{-2}$ and $D = 20\,\mathrm{s}^{-1}$. The significant improvements of the end-effector position error norm within Fig. 7a) demonstrate the potential of the applied feedback controller in combination with the nonlinear state estimator. This also confirms that the estimated signals are suitable for feedback control. Moreover, similar to the changes of the errors, the actuator position corrections can make up to few centimeters. In Fig. 7b) the positive effect of the controller can be seen especially at the trajectory end at which the overshoot is significantly decreased.

6. CONCLUSIONS

A nonlinear state estimator based on an Unscented Kalman Filter algorithm is applied to a manipulator with a highly flexible link and a kinematic loop, using actuator position and strain measurements. Here, the arising differential

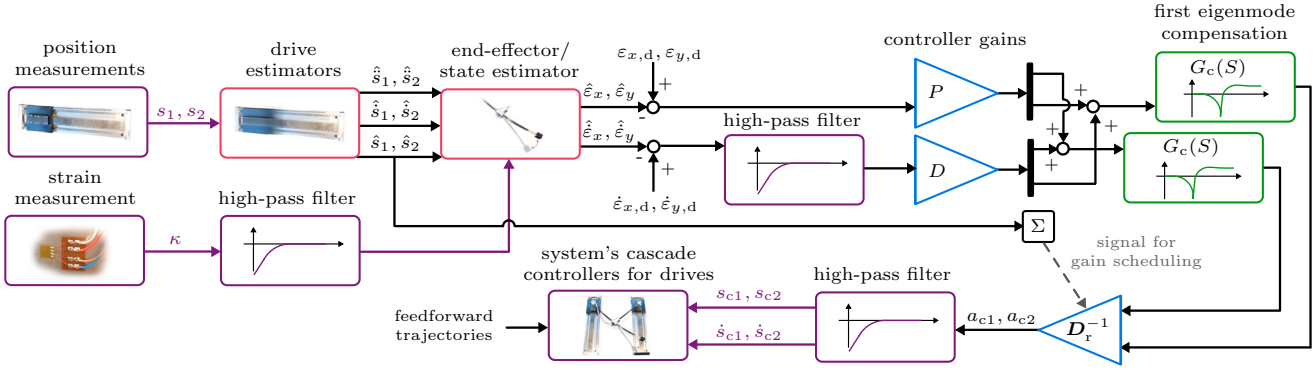

Fig. 6. Control structure of the estimators combined with the end-effector feedback controller.

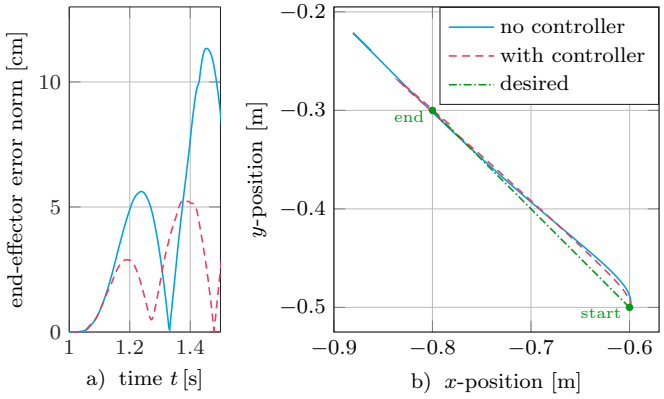

Fig. 7. Estimated a) Euclidean end-effector trajectory tracking error norm and b) path plots for the line trajectory with and without end-effector feedback control.

algebraic equations are treated by projections tangential to the constraint manifold. The corresponding end-effector estimation is then utilized within a feedback controller which is based on inverse kinematics of an equivalent rigid model with an additional compensation of the first bending eigenmode. The experiments show a significant improvement of the end-effector trajectory tracking.

The presented control approach is valuable to show some first end-effector feedback control results, but for a better performance more elaborate nonlinear control concepts need to be considered which can be combined with the developed estimator. Besides, it will be investigated how model adaptions and a real-time capable camera for direct measurements can improve the end-effector estimation.

ACKNOWLEDGEMENTS

The authors thank Professor Peter Eberhard for providing the experimental rig at the Institute of Engineering and Computational Mechanics at the University of Stuttgart.

REFERENCES

Burkhardt, M., Holzwarth, P., and Seifried, R. (2013). Inversion based trajectory tracking control for a parallel kinematic manipulator with flexible links. In Z. Dimitrovová (ed.), *Proc. of the 11th Int. Conf. on Vibration Problems, Lisbon, Portugal*.

Burkhardt, M., Seifried, R., and Eberhard, P. (2015). Experimental studies of control concepts for a parallel manipulator with flexible links. *J. of Mechanical Science and Technology*, 29(7), 2685–2691.

Hairer, E., Lubich, C., and Wanner, G. (2006). *Geometric Numerical Integration - Structure-Preserving Algorithms for Ordinary Differential Equations*. Springer Berlin Heidelberg New York, 2 edition.

Marafioti, G., Olaru, S., and Hovd, M. (2009). State estimation in nonlinear model predictive control, unscented kalman filter advantages. In *Nonlinear Model Predictive Control*. Springer.

Morlock, M., Burkhardt, M., and Seifried, R. (2016). Control of vibrations for a parallel manipulator with flexible links — concepts and experimental results. *Journal of Physics: Conference Series*, 744, 012069.

Morlock, M.B., Burkhardt, M., and Seifried, R. (2015). Friction compensation, gain scheduling and curvature control for a flexible parallel kinematics robot. In *IEEE/RSJ Int. Conf. on Intelligent Robots and Systems*, 2354–2359.

Pastorino, R., Richiedei, D., Cuadrado, J., and Trevisaniolzorlock, A. (2013). State estimation using multibody models and non-linear Kalman filters. *International Journal of Non-Linear Mechanics*, 53, 83–90.

Seifried, R. (2014). *Dynamics of Underactuated Multibody Systems*. Springer.

Seifried, R., Burkhardt, M., and Held, A. (2013). Trajectory control of serial and parallel flexible manipulators using model inversion. In J. Samin and P. Fisette (eds.), *Multibody Dynamics: Computational Methods and Applications, Computational Methods in Applied Sciences*, volume 28, 53–75. Springer.

Shabana, A.A. (1997). Flexible multibody dynamics: review of past and recent developments. *Multibody System Dynamics*, 1(2), 189–222.

Singer, R.A. (1970). Estimating optimal tracking filter performance for manned maneuvering targets. *IEEE Transactions on Aerospace and Electronic Systems*, AES-6(4), 473–483.

Teixeira, B.O., Chandrasekar, J., Tôrres, L.A., Aguirre, L.A., and Bernstein, D.S. (2009). State estimation for linear and non-linear equality-constrained systems. *International Journal of Control*, 82(5), 918–936.

Thrun, S., Burgard, W., and Fox, D. (2005). *Probabilistic Robotics*. The MIT Press.

Wan, E.A. and Van Der Merwe, R. (2000). The unscented Kalman filter for nonlinear estimation. In *Proc. of the IEEE 2000 Adaptive Systems for Signal Processing, Communications and Control Symposium*, 153–158.